Photocatalytic aqueous succinic acid production by maleic acid reduction

Marianna Bellardita*, Danilo Virtù, Francesco Di Franco, Vittorio Loddo,

Leonardo Palmisano, Monica Santamaria*

Dipartimento di Ingegneria, Università degli Studi di Palermo, Viale delle Scienze Edificio 6, 90128, Palermo, Italy.

Corresponding authors: Marianna Bellardita (marianna.bellardita@unipa.it), Monica Santamaria (monica.santamaria@unipa.it).

Abstract

This study reports the anaerobic reduction of maleic acid to succinic one in aqueous dispersion of different TiO_2 based photocatalysts. Some home prepared and commercial solids containing different polymorphic phases of TiO_2 and loaded with Pt and Ru were compared at different acidic pHs. The aim of the work was to determine the effectiveness of the process, the best samples, and the optimal experimental conditions of the reaction. The best selectivity towards succinic acid was 23.2 % at 70 % of maleic acid conversion. Fumaric acid was also formed as another high added value compound.

Keywords: photocatalytic synthesis, high added value chemicals, maleic acid reduction, succinic acid production, TiO_2.

Introduction

Succinic acid (SA) is a dicarboxylic acid containing four-carbon atoms (HOOC-CH_2-CH_2-COOH), which has attracted great interest due to its employment as a precursor for many industrially important chemicals in pharmaceutical, chemical and food industries [1]. In particular, recently has been used in the synthesis of

biodegradable polymers such as polyamides, butylene succinic acid, polybutyrate succinate [2,3] and has been included by the USA Energy Department in the "Top 10" list of biomass-derived compounds [4]. Traditionally, succinic acid is obtained industrially through the catalytic hydrogenation of maleic anhydride or maleic acid (MA) [5]. Faced with the depletion of crude oil reserves, the inconvenient related to chemical methods, and the affirmation of eco-sustainable processes, valid alternative ways of synthesis are represented by biological, electrochemical and photocatalytic processes [6-12] which are competitive in terms of cost, environmental impact and performance. The biological methods involve the production of succinic acid by fermentation starting from various precursors (glucose, xylose, glycerol, maleic or fumaric acid) and different microorganism types [1,13]. Pinazo et al. [6] compared the production of succinic acid from biomass-based compounds via fermentative synthesis and petrochemical routes by considering four parameters: (i) energy efficiency; (ii) economics; (iii) material efficiency; (iv) land use. The biological synthesis displayed a slightly higher energy efficiency, moderately lower costs and a rather lower material efficiency than the petrochemical way. Although it is environmentally benign, the biological method presents some weaknesses, in fact the productivity is of the order of a few g l^{-1} h^{-1} and the formation of by-products requires the recovery and the purification of the main product. Several electrochemical studies have been carried out starting from maleic acid under different experimental conditions [8,9,14,15]. The reduction/hydrogenation reaction of maleic acid to succinic one has been studied by varying the type of cathode, the electrolyte (aqueous acidic, neutral and alkaline media or organic solvents), the presence of cell separators, the current density, and the temperature. Generally, high succinic yield values (>85%) and current efficiencies (80%) were observed being the highest values obtained at low pH values (ca. 2) by H_2SO_4 addition and by using TiO_2 based cathodes [8,15]. Other metallic cathodes, as those consisting of lead, displayed good performance but they are expensive, noxious for the environment and can contaminate the products. Moreover, other factors as the necessity of the addition of a supporting electrolyte in the cell and the high cost of the catalysts, limit the viability of this process.

TiO_2, in addition to being a very promising materials in electrocatalysis due to its high stability and redox selectivity [16,17] is the most used photocatalyst [18,19] with a good activity in reduction reactions [20-22].

The photocatalytic hydrogenation of organic substrates deriving from biomass, or other waste products, in aqueous solvents and under mild experimental conditions, represents a valuable alternative to catalytic methods. In this context, the photocatalytic hydrogenation of maleic acid to succinic acid is a very interesting process which has been little studied. Succinic acid has been obtained photocatalytically as a by-product during the aerobic oxidation of maleic acid (MA) [23] and as a target compound during the anaerobic reduction of maleic acid [11] and fumarate [12]. Hu et al. [11] carried out the hydrogenation of maleic acid under simulated solar light irradiation in the presence of H_2O as the solvent, ascorbic acid as holes trap and a metal-free thiophene-containing covalent triazine polymer (home-made prepared) as photocatalyst. Only succinic acid has been identified as reaction product with a production rate of 2 mmol g^{-1} h^{-1} at pH = 2.

Another study has been presented by Zhou et. al [12] who used colloidal ZnS suspended in water in the presence of different amounts of Na_2S as hole scavenger to study the surface photoprocesses during the reduction of fumarate to succinate. However, they only verified the formation of succinic acid without quantifying it.

In this study we report the anaerobic reduction of maleic acid in acidic aqueous solution using different TiO_2-based photocatalysts. In particular, samples containing different polymorphic forms of TiO_2, loaded with Pt and Ru, at different pH values were compared. Pt is one of the most active metals used for H_2 production under reducing conditions [24] while Ru was chosen as it reduces the poisoning of the catalyst surface due to CO [25]. The aim of this work was to verify the effectiveness of the process and to identify the most efficient samples and the best experimental conditions of the reaction. Generally, it is not easy to obtain acceptable selectivity values during partial photocatalytic reduction reactions in the presence of water alone as a solvent.

2. Experimental

2.1 Samples preparation

Titanium tetrachloride ($TiCl_4$ Sigma-Aldrich 98%), titanium(IV) isopropoxide (TTIP, Aldrich ≥97%), ethanol (Sigma-Aldrich), HCl (Sigma-Aldrich 37%), Pluronic P127 (Sigma-Aldrich), $PtCl_4$ (BDH Chemicals) and $RuCl_3$·hydrate (Sigma-Aldrich) were used as received for the synthesis of different TiO_2 based photocatalysts. Commercial BDH and Aeroxide P25 TiO_2 samples were used for the sake of comparison and have been indicated as BDH and P25.

Brookite TiO_2 was obtained by the hydrothermal hydrolysis of $TiCl_4$ in HCl aqueous solutions [26]. In particular, 10 mL of $TiCl_4$ were slowly added under stirring to a solution containing 420 mL of water and 160 mL of concentrated HCl. Then the solution was transferred in a Pyrex bottle and heated at 373 K for 48 h. A precipitate containing a brookite/rutile mixture was obtained. Brookite was separated by peptization adding water at different time, and removing the supernatant were brookite was selectively dispersed. This sample was labelled as Brookite.

A sample consisting of pure rutile (code Rutile) was prepared by adding 10 mL of $TiCl_4$ to 50 ml of distilled water under stirring at room temperature. The obtained solution was placed in a Pyrex bottle, closed and treated at 373 K in an oven for 48 h. The solid was recovered by drying under vacuum at 323 K.

Another photocatalyst was synthesized by adding TTIP to an aqueous solution containing ethanol, chloridric acid and Pluronic P127 as surfactant. The molar ratio between the used reagents was: TTIP (1) : H_2O (15) : C_2H_5OH (40) : HCl (0.5). The gelatinous dispersion obtained was stirred at ambient temperature for 48 h, successively the solvent was evaporated and the recovered solid was calcined at 773 K for 24 h. This sample was named as AR.

TiO_2 samples were loaded with 0.5% wt of Pt and/or 0.5% of Ru by the photodeposition method using $PtCl_4$ and $RuCl_3 \cdot 2H_2O$. 200 mL of H_2O, 50 mL of ethanol, 1 g of TiO_2 and the proper amount of the metals precursors were added to a 500 mL Pyrex photoreactor. Helium was bubbled for 30 minutes under dark to deaerate the solution and for ca. 8 h under irradiation to allow the deposition of the two metals. The powders were recovered by evaporating the solution at 253 K. The codes used for these samples were the same as that of the corresponding pristine TiO_2 preceded by the name of the metal(s).

A catalyst containing both rutile and brookite (Pt-RB) was obtained by aging the sample Pt-Rutile for 3 years at room temperature. Probably, a part of the amorphous phase present in the sample was transformed into brookite phase after a so long time. However, it is not aim of this paper to deepen the study of the material.

2.2 Samples characterization

X-Ray diffraction (XRD) patterns of the samples were acquired at room temperature by a PANalytical Empyrean diffractometer equipped with a PIXcel^{1D} (tm) detector working at a voltage of 40 kV and a current of 40 mA and using the CuKα radiation and a 2θ scan rate of 1.28 °/min.

Raman spectra were recorded employing a BWTek-i-micro Raman Plus System, equipped with a 785 nm diode laser. The spectra were collected in the 125-1000 cm^{-1} Raman shift range and every measure was the average of two repetitions.

The specific surface areas (SSA) of the powders were measured by a Flow Sorb 2300 apparatus (Micromeritics) by using the single-point BET method. The samples were degassed for 30 min at 523K before the measurement.

The optical properties of the samples were studied by UV-Vis spectroscopy. The Diffuse Reflectance Spectra (DRS) were acquired at room temperature in the 200-800 nm wavelength range by using a Shimadzu UV-2401 PC spectrophotometer. $BaSO_4$ was used as the reference sample. Band gap values were calculated by plotting the modified Kubelka-Munk function, $[F(R'_\infty)hv]^{1/2}$, versus the energy of the exciting light.

Scanning electron microscopy (SEM) images were obtained by using a FEI Quanta 200 ESEM microscope operating at 30 kV on specimens upon which a thin layer of gold was deposited. An electron microprobe used in an energy dispersive mode (EDX) was used to obtain information on samples composition.

2.3 Photocatalytic tests

The photoreactivity experiments were carried out by using different TiO_2 based samples both commercial, i.e., Aeroxide P25 and BDH, and home-prepared. The runs were performed in a cylindrical Pyrex reactor containing 150 mL of an aqueous dispersion, irradiated by a 125 W medium pressure Hg lamp whose main emission peak was at 365 nm. Nitrogen was bubbled in the suspension for 0.5 h under dark condition, then the reactor was closed and the lamp switched on. Water was circulated through a Pyrex thimble to keep the temperature of the suspension at about 303 °C. The concentration of the catalysts was 0.6 g L^{-1} and the initial concentration of maleic acid (MA) was 1 mM. The "natural" pH of the SA solution after the addition of the different catalysts was ca. 2.6. By considering the results obtained in previous works [8,11], some runs were carried out by decreasing the pH of the dispersion down to 2 or 1 by using 1 M H_2SO_4 or HCl solutions.

Samples of the irradiated solution were withdrawn at fixed times and filtered through 0.2 µm PTFE membranes to separate the catalyst particles. The quantitative determination of maleic acid and the reaction intermediates was made through a Thermo Scientific Dionex UltiMate 3000 HPLC equipped with a Diode Array detector equipped with a REZEK ROA Organic acid H^+ column. The eluent used was an aqueous 2.5 mM H_2SO_4 solution at a flow rate of 0.6 mL·min^{-1}. The different species were identified by comparing their retention times and their UV–Vis spectra with those of standards. The gaseous species accumulated in the reactor headspace were withdrawn by a 500 µL gas-tight syringe and analysed by an HP 6890 Series GC System equipped with a Supelco GC 60/80 Carboxen^{TM}-1000 packed column and a thermal conductivity detector.

Results and Discussion

In Figure 1 the X-ray diffraction patterns of the different photocatalysts with the indication of the characteristic peaks of the three main TiO_2 polymorphs are reported. For all of the samples are also showed the diffractograms collected in the presence of Pt/Ru as no differences were noticed in comparison with the naked correspondent powders (Figure 1b). The peaks at 2θ = 25.5°, 38.0°, 48.0°, 54.5° are characteristic

of Anatase, those at 2θ = 27.5°,36.5°, 41°, 54.1°, 56.5° of Rutile, and those at 2θ = 25.34°, 25.69◦, 30.81° of Brookite. The commercial samples BDH and P25 consist of Anatase and a mixture of Anatase and Rutile, respectively. The homemade photocatalysts show the different phases of TiO_2: Brookite (Pt-Brookite), Rutile (Pt-Rutile), a mixture of Anatase and Rutile (Pt-AR), and a mixture of Rutile and Brookite (Pt-RB). The peaks of the commercial photocatlysts are more intense than those of home-made ones, indicating a greater crystallinity of the former due to the high temperature reached during their preparation. The presence of photodeposited metals was not detected due to its low amount and high dispersion on the catalyst's surface. In fact, no shifts in the diffractograms lines were detected with respect to the bare samples. In Figure 1b the diffractrograms of bare and metal loaded BDH are compared and not differences due the metals presence can be observed.

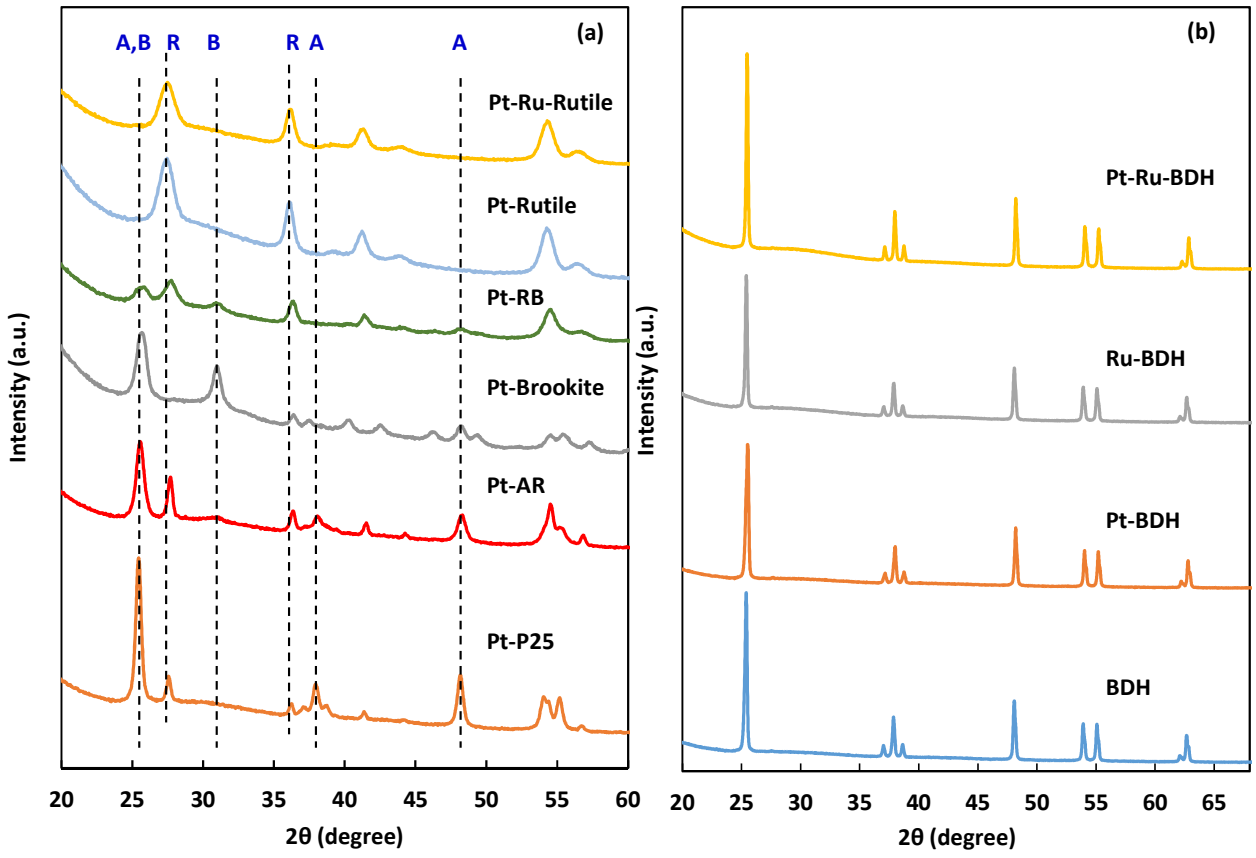

Figure 1: XRD patterns of the used samples. A = Anatase; R = Rutile; B = Brookite.

In Table 1 some properties of the used samples are reported. The specific surface areas (SSA) of the commercial solids are lower than those of the homemade ones, being 10 $m^2 \cdot g^{-1}$ for Pt-BDH and 50 $m^2 \cdot g^{-1}$ for Pt-P25. Values ranging from 73 $m^2 \cdot g^{-1}$ to 85 $m^2 \cdot g^{-1}$ were measured for the home-made photocatalysts.

Nominal M/Ti % weight percentage was 0.8 whilst the Pt/Ti and Ru/Ti atomic percentages were 0.2 and 0.4, respectively. The EDAX analysis confirmed the presence of both metals and the figures were approximately very close to the nominal ones, by considering the average values of the measurements repeated in three different places of the particles.

Table 1. Some features of the used samples.

Sample	**Crystalline phase**	**S.S.A. (m^2 g^{-1})**	**Band gap (eV)**
BDH	A	10	3.24
Pt-BDH	A	10	3.26
Ru-BDH	A	10	3.31
Pt-Ru-BDH	A	9	3.30
Pt-Rutile	R	85	2.98
Pt-Ru-Rutile	R	75	2.85 (2.20)
Pt-Brookite	B	83	3.34
Pt-P25	A,R	50	2.96
Pt-AR	A,R	73	2.92
Pt-RB	R,B	76	3.05
Pt-Ru-RB	R,B	65	2.76 (2.18)

SEM images (Figure 2) revealed that the different photocatalysts consist of aggregates of irregular spherical small particles which dimensions ranging between 100 and 500 nm. The particles size of home-made samples are smaller than those of commercial ones, due the lower synthesis temperature.

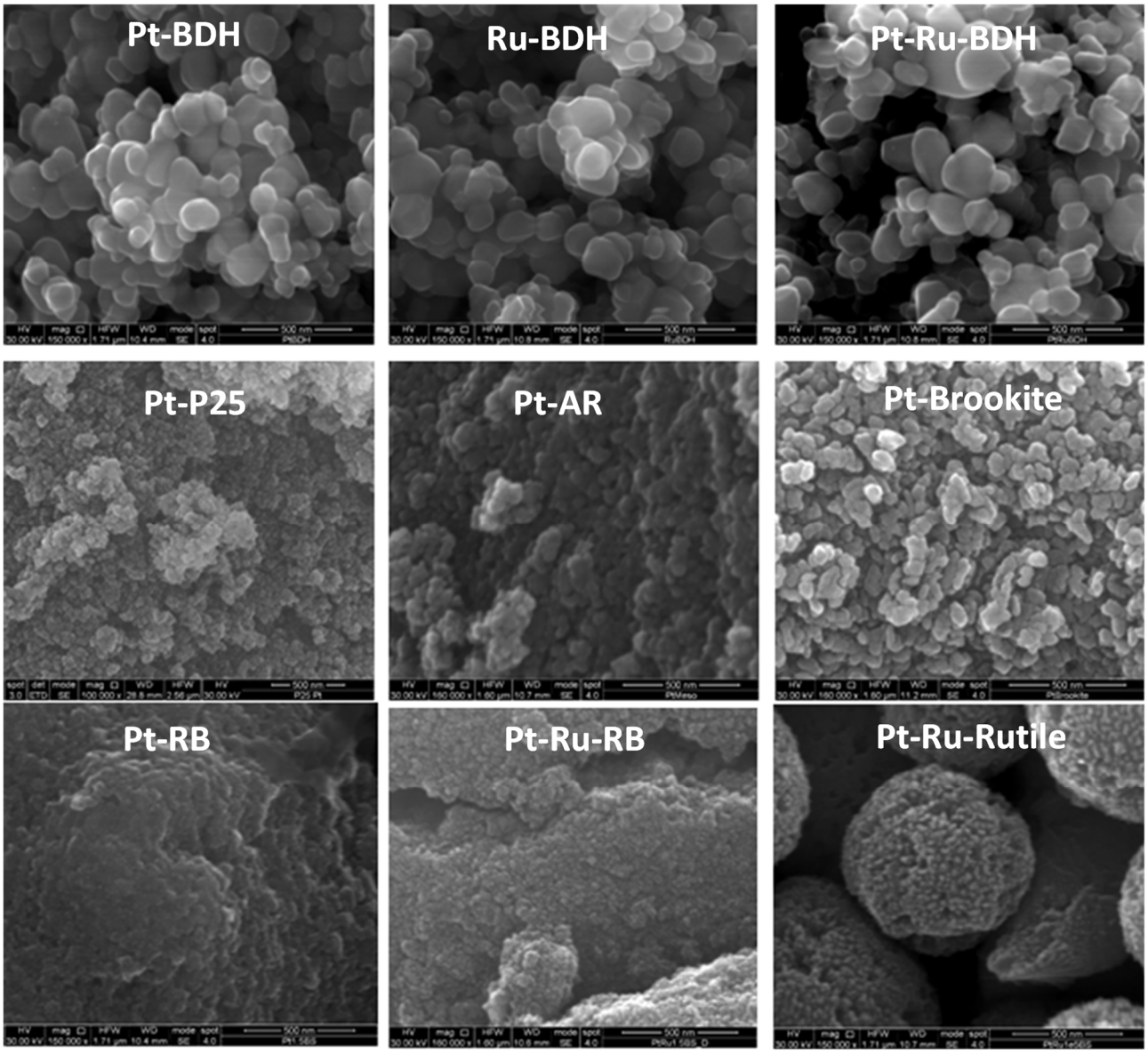

Figure 2: SEM images of the various samples.

Figures 3a and 3b show the diffuse reflectance (DRS) spectra of the different TiO_2 based samples. Commercial BDH sample displays an absorption band in the high energy region (λ < 360 nm) typical of Anatase ad attributed to the band-to-band transition. All of the other samples, with exception of Brookite, show a slight shift in absorption towards higher wavelengths, and the variation is more evident for Pt-P25 and Pt-AR. In the presence of the metals, it can be observed a lower reflectance value but no substantial variations in the absorption edges. The TiO_2 photocatalysts are all active under UV-visible light irradiation displaying band gap values that range between 3.34 and 2.76 eV (Table 1).

In Figure 3 (b) the DRS spectra of home-made samples containing Rutile as the main or single phase are presented. When only Pt is deposited on the surface of these catalysts, a single absorption edge typical of TiO_2 Rutile is observed, while when also Ru is present, another absorption edge is shown at about 550 nm. As can be seen from the Tauc graph in the inset of Figure 3(b), it is possible to calculate two band gap values, one at 2.85 eV due to Rutile and another at 2.20 eV, attributed to RuO_2 [27].

The presence of the two absorption edges is indicative of the formation of a heterostructure between ~~TiO_2~~ and RuO_2 [27-29]. This result is surprising both because when the hosted oxide is present in small quantities it is not detected with spectroscopic methods and the temperature reached during the preparation of the composite material is not very high.

Similarly to Pt, a photodeposition method in a reducing environment was used to obtain Ru in the metallic state, starting from $RuCl_3$ (see experimental section). The formation of an oxide generally requires treatments at high temperatures and the presence of oxygen, while in this case the powders were simply dried at 253 K after the photodeposition treatment in a deaerated solution to evaporate the solvent. Furthermore, since the formation of RuO_2 is characteristic of home-made samples (Rutile and Rutile-Brookite mixture), it may be due to some of their structural and surface characteristics compared to commercial BDH TiO_2 which consists of pure Anatase. Most likely, in fact, fundamental roles are played both by the structural characteristics of the Rutile phase itself and by its surface acidity which is higher than that of BDH, due to the precursor used during the synthesis procedure. Notably, samples prepared starting from $TiCl_4$ displayed a much lower zero charge point than the commercial ones [30]. Due to the similar lattice parameters of TiO_2 rutile and RuO_2, the dispersion capacity of the latter on Rutile is higher than on Anatase [31], and probably also the crystallization of RuO_2 could be favoured on the surface of Rutile compared to that of Anatase. Moreover, the specific surface area of Rutile is higher than that of Anatase facilitating the dispersion of RuO_2.

RuO_2 (nominal RuO_2 loading amount 0.01, 0.1, 0.25, and 0.5 wt %) was coupled with Rutile by impregnation of bare TiO_2 with $RuCl_3 \cdot xH_2O$ solutions and subsequent calcination in air at 473K for 2 h [32]. No peaks ascribable to RuO_2 were observed in both XRD patterns and Raman spectra, whereas a red shift and a

broadening of rutile Raman feature at 448 and 615 cm^{-1} were, instead, observed. In accordance with Parker and Siegel [33], for Rutile, the Raman bands shift toward lower wavenumbers, is characteristic of an increase of oxygen vacancy defects. In this case, the alteration of oxygen amount was attributed to the Schottky heterojunction at the interface between RuO_2 and TiO_2.

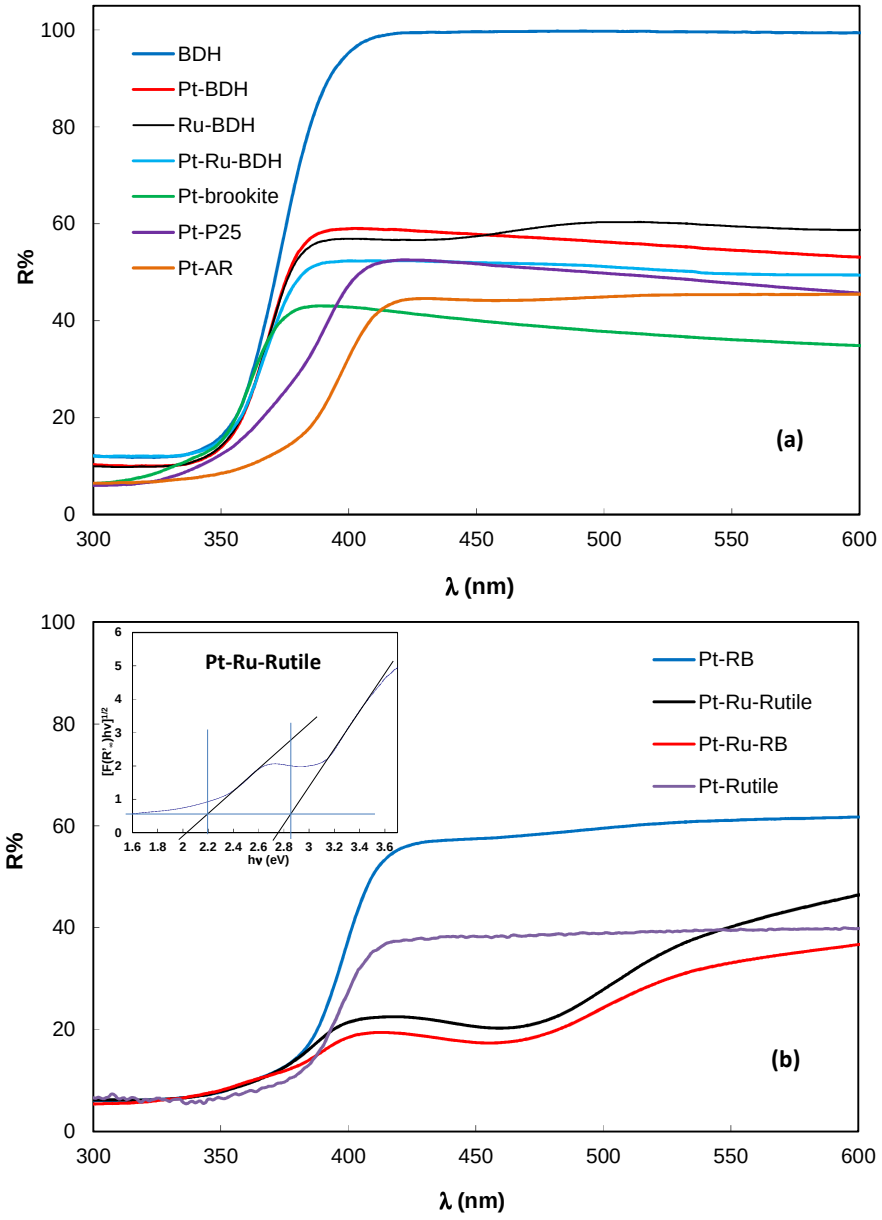

Figure 3: DRS spectra of the various samples. In the inset of Figure (b) is reported the Tauc Plot of the sample Pt-Ru-Rutile.

In Figure 4(a) the Raman spectra of commercial pristine and loaded BDH samples are reported. The characteristic modes of Anatase at 144 cm^{-1} (Eg), 196 cm^{-1} (Eg), 397 cm^{-1} (B1g), 513 cm^{-1} (A1g), and 639 cm^{-1} (B1g) [34] are highlighted. The presence of the metal species causes a decrease of the bands' intensity that can be associated with the greater surface disorder when Pt or Ru are present on TiO_2. Additionally, in the Pt-Ru-BDH sample two new bands appear at ca. 448 and 600 cm^{-1}, that practically coincide with the main Rutile modes at 447 (Eg) and 612 (A1g) cm^{-1} but most likely could be due to hydroxylated species of ruthenium. In fact, the presence of Rutile is improbable as it would mean to transform a small fraction of Anatase into Rutile at low temperature in a very crystalline commercial sample. Furthermore, the presence of Rutile has not been found in the diffractograms. No shifts in the Anatase peaks can be observed after Pt/Ru deposition. This is in accordance with their presence on the surface and the non-introduction of metals into TiO_2 lattice.

As far as the Rutile TiO_2 sample is concerned (Figure 4b), no variations in the Raman spectrum were observed in the presence of Pt, whilst some new bands are visible in the presence of Ru. The mode at ca. 500 cm^{-1} [31] can be attributed to RuO_2 in accordance to the reflectance spectrum, the others could be due to Ru hydroxylated species.

In the other samples, the addition of Pt does not introduce new bands with respect to the naked photocatalysts.

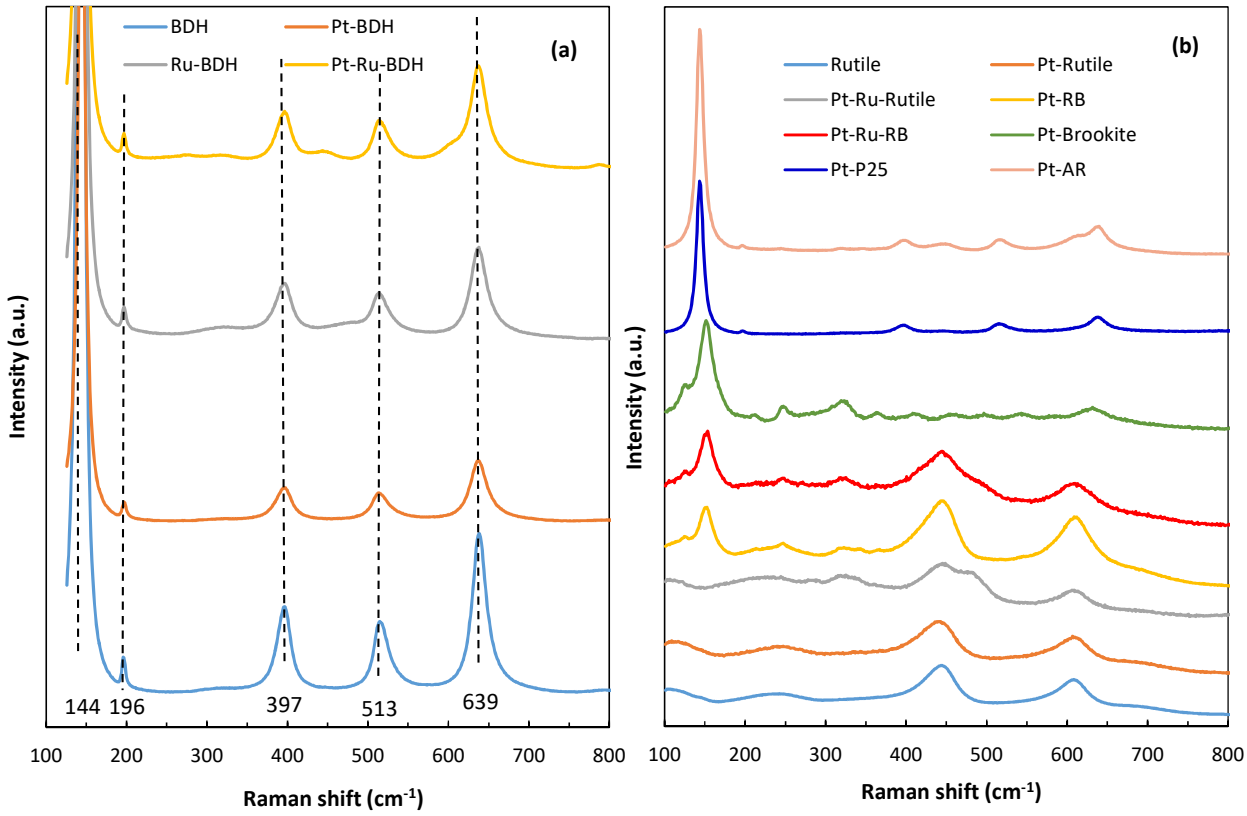

Figure 4: Raman spectra of the used samples.

In Table 2 the results of the photocatalytic runs carried out at pH = 2 are presented in terms of conversion of MA and selectivity towards the main reaction intermediates. No SA was obtained in the open reactor and in the absence of Pt. As SA can be formed from MA by a reduction reaction, the presence of Pt and anaerobic conditions were essential, in accordance with the literature [11,22]. Good SA production values were found at pH = 2 both by electrocatalysis [8] and photocatalysis [11], and consequently in this work a preliminary screening was carried out by comparing the different samples at this pH by adding H_2SO_4 to decrease the "natural" one of the MA solution (2.6). In addition to SA, the main reaction intermediates identified were fumaric acid (FA), malonic acid (MalA), acrylic acid (AA), and traces of unknown compounds were also present. The presence of platinum on the surface of the catalysts had a beneficial effect both on the conversion of MA and the formation of SA. The metal, in fact, acting as an electron attractor, prevents the recombination with holes and makes them more readily available for the reduction of MA to SA. At pH

= 2 by H_2SO_4, the highest conversion values were obtained with Pt-BDH and Pt-AR samples. To study the influence of different acids, some runs were carried out by adjusting the pH value to 2 by HCl addition. In the latter case, two opposite behaviours were noticed by comparing the results obtained with Pt-P25 and Pt-BDH with those achieved in the presence of H_2SO_4, in fact, in the presence of HCl the selectivity and the activity increased by using Pt-P25 and decreased with Pt-BDH. In both cases, however, low selectivity values to SA (<4%) were obtained.

Table 2. Results obtained after 6 hours of irradiation of for runs carried out at pH = 2. X = conversion, S = selectivity. MA (maleic acid); SA (succinic acid); FA (fumaric acid); MalA (malonic acid); AA (acrylic acid).

Sample	**Acid**	**X (MA) %**	**S (FA) %**	**S (SA) %**	**S (MalA) %**	**S (AA) %**
BDH	H_2SO_4	23.5	10.7	-	-	-
Pt-BDH	H_2SO_4	88.0	0.6	4.4	18.0	-
Pt-P25	2.6 without acid	96.0	0.8	-	-	3.1
Pt-P25	H_2SO_4	84.5	14.6	trace	6.3	2.3
Pt-AR	H_2SO_4	91.5	17.0	-	8.7	0.9
Pt-RB	H_2SO_4	82.0	31.8	7.3	5.7	0.3
Pt-P25	HCl	91.7	0.7	2.1	-	1.0
Pt-BDH	HCl	79.3	5.1	3.8	3.2	1.4

In order to enhance the efficiency of the process, the pH of the reaction mixture was further decreased to 1, and also in this case a comparison between H_2SO_4 and HCl was made (Table 3). By diminishing the pH better performances were achieved. For Pt-BDH in the presence of H_2SO_4 the MA conversion increased from 88 to 95.5 % and the selectivity to SA from 4.4 to 5.2 % while by adding HCl the conversion was 96.4 % and the selectivity reached 7.6 %. Accordingly, the subsequent runs were carried out by lowering the pH to 1 utilizing HCl (Figure 5).

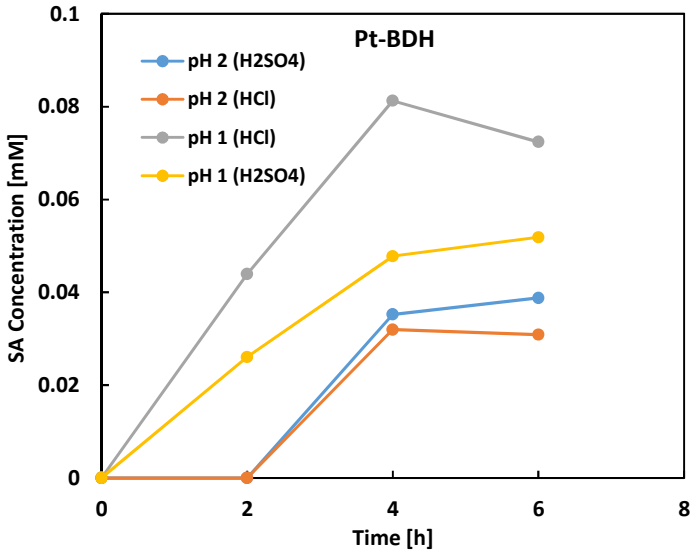

Figure 5: Succinic acid concentration versus time in different experimental conditions.

To be sure that oxygen is almost completely removed from the reaction environment, a test was performed with Pt-BDH by opening the reactor and bubbling N_2 over the irradiation time. In this condition, the MA conversion was the same than that in the closed reactor, but the selectivity towards SA decreased. Therefore, the subsequent runs were carried out maintaining closed the reactor after N_2 bubbling for 30 minutes. Since brookite and rutile showed good reduction performances in a previous study [22], these two polymorphs, alone or in mixture, were used under the optimized conditions. High conversion values were obtained with almost all the samples, while different selectivity values and a different distribution of the reaction intermediates were observed with the different photocatalysts used. In the presence of platinum alone, the home-prepared catalysts were more active than the commercial BDH sample. Rutile showed a lower oxidant capability than BDH being the MA conversion 78.6 % and brookite, generally not very active in oxidation reactions, allowed 93.4 % of conversion with, however, a lower selectivity than rutile (7.9 % versus 21.1 %). The activity of the rutile-brookite mixture (Pt-RB) was worse than that of the single oxides, even though, generally, the heterojunction between two semiconductors has a beneficial effect on the separation of the photogenerated charges and therefore on the activity. The addition of Ru alone had a negative effect on the photoactivity of the BDH, while a significant improvement was observed on this

sample in the presence of both metals. In fact, the selectivity value was more than twice compared to that found in the presence of the Pt loaded sample. This behaviour can be due to a synergistic effect between the two metals and the BDH surface. An opposite result was observed on Rutile as the simultaneous presence of the two metals led to a decrease of both the substrate conversion and the selectivity to succinic acid. Most likely the two metals interact differently with the surface of the two phases of TiO_2, in accordance with DRS and Raman. Moreover, Anatase and Rutile phases have different physico-chemical properties that could affect type and degree of catalyst-substrate interaction and, consequently, the photocatalytic activity [35]. In particular superficial Ru is present in the metallic form on anatase, whilst formation of RuO_2 was detected in the presence of rutile. This finding can explain the higher photoactivity of Pt-Ru-BDH sample with respect to Pt-Ru-Rutile in a reducing environment. On the other hand, RuO_2 is not beneficial, on Rutile, probably because its conduction band edge (0.76 V) [27] is more positive than that of TiO_2 (CB edge ranging between -0.37 and -0.46 V, depending on the polymorphic form) [36], being the reduction potential of maleic acid 0.21 V [11].

Table 3. Runs carried out at pH=1. Results obtained after 6 h of irradiation. X = conversion, S = selectivity. MA (maleic acid); SA (succinic acid); FA (fumaric acid); MalA (malonic acid); AA (acrylic acid).

Sample	**Acid**	**X (MA) %**	**S (FA) %**	**S (SA) %**	**S (MalA) %**	**S (AA) %**
Pt-BDH	H_2SO_4	95.5	0.1	5.2	15.4	-
Pt-BDH	HCl	96.4	15.3	7.6	1.7	-
Pt-BDH (N_2)	HCl	96.4	22.5	3.8	-	-
Pt-Rutile	HCl	78.6	15.0	21.1	4.7	1.5
Pt-RB	HCl	73.0	37.4	11.2	-	0.6
Pt-Brookite	HCl	93.4	26.7	7.9	1.8	1.6
Ru-BDH	HCl	32.9	26.6	-	-	1.3
Pt-Ru-BDH	HCl	92.8	10.3	20.5	4.5	0.7
Pt-Ru-Rutilo	HCl	47.3	12.0	8.1	-	1.5

In order to allow a more direct comparison between the different samples, the selectivity towards SA was calculated at the same value of alcohol conversion (70%) and reported in Figure 6. The highest value (23.3 %) was obtained for Pt-Ru-BDH followed by Pt-Rutile.

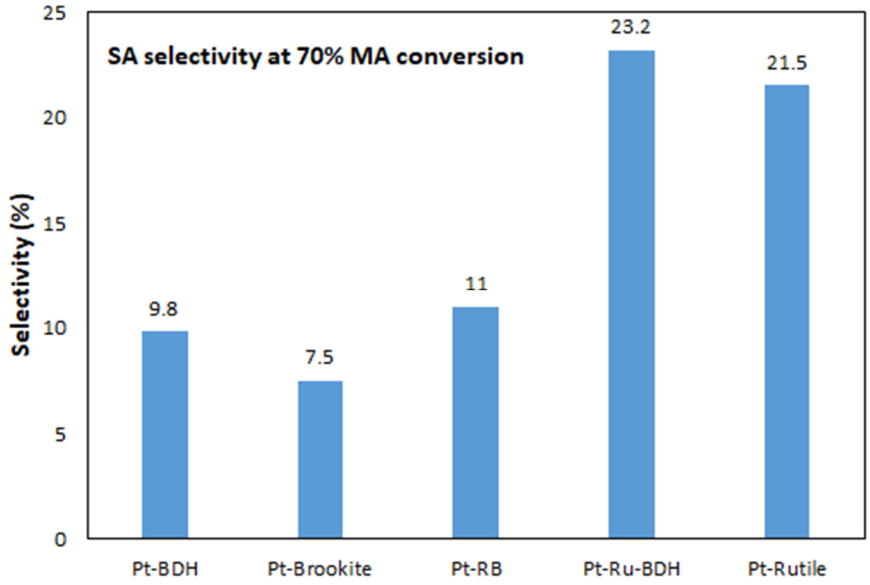

Figure 6: Succinic acid selectivity after 70% conversion of MA.

The major co-product of the reaction is FA, which is also a valuable compound being an important food additive and industrial intermediate [37]. It is produced by isomerization of maleic acid under high temperature and pressure conditions. Under the used experimental conditions, FA is obtained at pH = 1 with selectivity values ranging between 10.3 and 37.4 % in the presence of the different photocatalysts (Table 3), being the highest value reached with Pt-RB. It can be noticed that by using Ru-BDH, although the alcohol conversion is low, FA is practically the only formed intermediate product. Therefore, if FA is the target product, in the presence of Ru-BDH no further separation steps are necessary to recover it. By using the other photocatalysts, subsequent separation methods are necessary to obtain the two valuable compounds. The formation of different products, or a different distribution of the formed products, by starting from the same substrate in the presence of the various TiO_2 polymorphs has been already observed during the partial oxidation of glucose under both aerobic and anaerobic conditions [22]. Also in this latter

case the highest formation of the glucose isomer (fructose) was obtained with the commercial anatase (TiO_2 BDH) photocatalyst although the two compounds are not geometric isomers but isomers of position. This finding has been attributed to the different surface properties of the different samples and in particular to the high Lewis acid centers concentrations on the anatase surface. In addition, the *cis-trans* photocatalytic isomerization is a well known process [38-41] and was explained with different mechanisms as reductive electron transfer [38] or energy transfer [39], although the occurrence of both mechanism cannot be ruled out.

In Scheme 1 a hypothesized sketch of the photocatalytic transformation of MA is reported. The initial step could be isomerization of MA to FA after the interaction of the substrate with the irradiated surface of the photocatalysts. Then the reaction of MA and FA with H^+ and electrons leads to the formation of SA through a reduction reaction [8]. One run was carried out at pH = 1 for HCl starting from FA with the sample Pt-RB and the formation of SA was confirmed. The interaction of MA with H^+, h^+ and $O_2^{\cdot-}$ gave rise to malonic and acrylic acids by an oxidation mechanism, in accordance with literature [41,42]. The analysis of the gaseous phase revealed the presence of small amounts of CO_2 deriving from the mineralization of the organic compounds, and in some cases only trace amounts of H_2, confirming that the main reducing pathway was the formation of SA. No light aliphatic species as acetic or formic acid were found. This finding suggests that, at least considering the time during which the reaction was carried out in this work, CO_2 results only from the breakdown of a terminal carbon atom of MA with the simultaneous formation of acrylic acid. In fact, by plotting the concentration of the different species versus the irradiation time (Figure 7) it can be observed that the concentration of the main intermediates (SA, MA, AA) continuously increases over time.

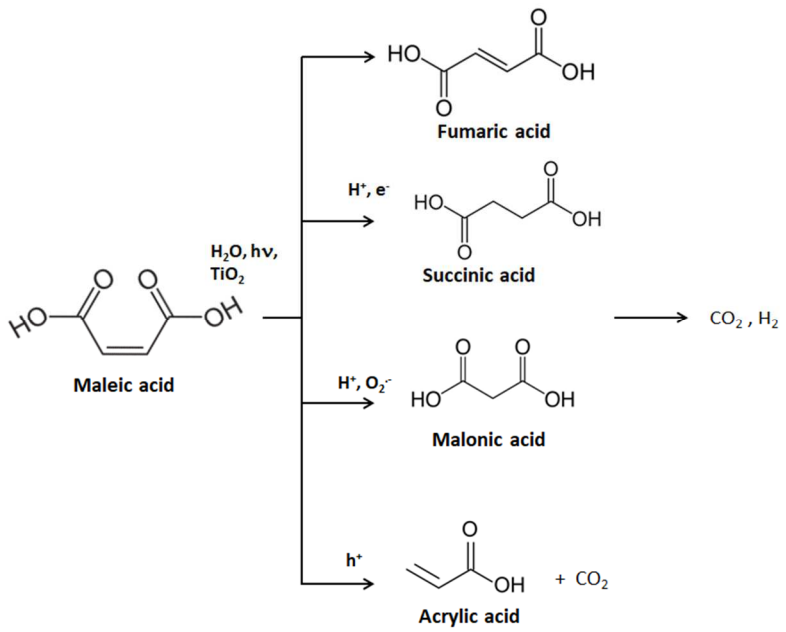

Scheme 1: Hypothesized sketch of the reaction pathway.

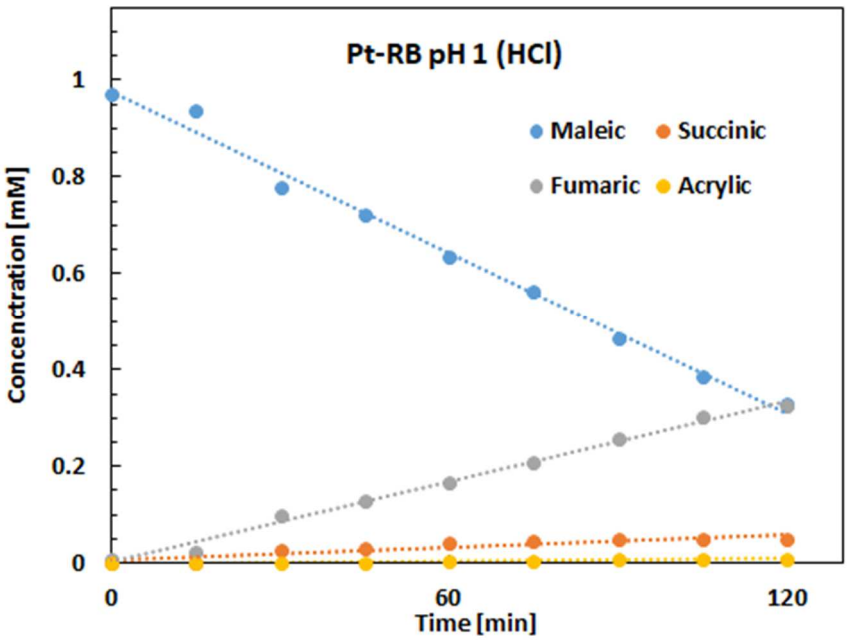

Figure 7: Variation of the concentration of MA, FA, SA and AA versus irradiation time.

Conclusions

The selective conversion of maleic acid to produce high added value compounds was carried out by means of heterogeneous photocatalysis under green experimental conditions by using different TiO_2 based photocatalysts. The presence of Pt resulted essential for the production of succinic acid. The highest selectivity values were obtained at pH = 1 by HCl addition. The addition of Ru was beneficial for BDH (Anatase) and detrimental for Rutile.

In the presence of various TiO_2 based photocatalysts a different distribution of the reaction products was obtained being the main products fumaric and succinic acid. Only fumaric acid, instead, was obtained with Ru-BDH.

References

[1] H. Song, S.Y. Lee, Production of succinic acid by bacterial fermentation, Enzyme Microbiol. Technol. 39 (2006) 352–361.

[2] T. Willke, K.-D. Vorlop, Industrial bioconversion of renewable resources as an alternative to conventional chemistry, App. Microbiol. Biotechnol. 66 (2004) 131-142.

[3] C. Delhomme, D. Weuster-Botz, F.E. Kühn, Succinic acid from renewable resources as a C4 building-block chemical – a review of the catalytic possibilities in aqueous media, Green Chem. 11 (2009) 13–26.

[4] J. Bozell, G. Petersen, Technology development for the production of biobased products from biorefinery carbohydrates—the US Department of Energy's "Top 10" revisited, Green Chem. 12 (2010) 539-554.

[5] B. Cornils, P. Lappe, Ullmann's Encyclopedia of Industrial Chemistry; Wiley-VCH Verlag: Weinheim, Germany (2010) 287–304.

[6] J.M. Pinazo, M.E. Domine, V. Parvulescu, F. Petru, Sustainability metrics for succinic acid production: A comparison between biomass-based and petrochemical routes, Catal. Today 239 (2015) 17-24.

[7] C. Pateraki, M. Patsalou, A. Vlysidis, N. Kopsahelis, C. Webb, A.A. Koutinas, M. Koutinas, Actinobacillus succinogenes: Advances on succinic acid production and prospects for development of integrated biorefineries, Biochem. Eng. J. 112 (2016) 285–303.

[8] D. Vasudevan, Medium effects in the electrosynthesis of succinic acid at a Ti/ceramic TiO_2 cathode, Russ. J. Electrochem. 45 (2009) 1310–1312.

[9] F. Zhao, F.Yan, Y. Qian, Y. Chu, C. Ma, Electrochemical synthesis of succinic acid at a TiO_2 film electrode orepared by in-situ anodic oxidation, Int. J. Electrochem. Sci. 7 (2012) 12931–12940.

[10] M. Suttipornphaisalkul, P. Wright, K. Kamwilaisak, Succinic acid production from lignin by photo-oxidation, Eng. Appl. Sci. Res. 47 (2020) 36-46.

[11] Y. Hu, W. Huang, H. Wang, Q. He, Y. Zhou, P. Yang, Y. Li, Y. Li, Metal-free photocatalytic hydrogenation using covalent triazine polymers, Angew. Chem. Int. Ed. 59 (2020) 14378–14382.

[12] R. Zhou, M. I. Guzman, Photocatalytic reduction of fumarate to succinate on ZnS mineral surfaces, J. Phys. Chem. C 120 (2016) 7349−7357.

[13] A. Kuenz, L. Hoffmann, K. Goy, S. Bromann, U. Prüße, High-level production of succinic acid from crude glycerol by a wild type organism, Catalysts 10 (2020) 470.

[14] A.V. Muzumdar, S.B. Sawant, V.G. Pangarkar, Reduction of maleic acid to succinic acid on titanium cathode, Org. Process Res. Dev. 8 (2004) 685-688.

[15] C.J. Kennedy, A.J. Reithinam, Thermally coated Ti/TiO_2 as cathode material for the synthesis of succinic and dihydrophthalic acids, J. Appl. Electrochem. 33 (2003) 831–834.

[16] B. Ren, Q. Jin, Y. Li, Y. Li, H. Cui, C. Wang, Activating titanium dioxide as a new efficient electrocatalyst: from theory to experiment, ACS Appl. Mater. Interfaces 12 (2020) 11607-11615.

[17] A. Lavacchi, M. Bellini, E. Berretti, Y. Chen, A. Marchionni, H.A. Miller, F. Vizza, Titanium dioxide nanomaterials in electrocatalysis for energy, Curr. Opin. Electrochem. 28 (2021) 100720.

[18] A. Fujishima, T.N. Rao, D.A. Tryk, Titanium dioxide photocatalysis, J. Photochem. Photobiol. C 1 (2000) 1-21.

[19] K. Nakata, A. Fujishima, TiO_2 photocatalysis: Design and applications, J. Photochem. Photobiol. C 13, (2012) 169-189.

[20] S.N. Habisreutinger, L. Schmidt-Mende, J.K. Stolarczyk, Photocatalytic reduction of CO_2 on TiO_2 and other semiconductors, Angew. Chem. Int. Ed. 52 (2013) 7372-7408.

[21] J. Yu, L. Qi, M. Jaroniec, Hydrogen production by photocatalytic water splitting over Pt/TiO_2 nanosheets with exposed (001) facets, J. Phys. Chem. C 114 (2010) 13118–13125.

[22] M. Bellardita, E. García-López, G. Marcì, L. Palmisano, Photocatalytic formation of H_2 and value-added chemicals in aqueous glucose (Pt)-TiO_2 suspension, Int. J. Hydrogen Energ. 41 (2016) 5934-5947.

[23] J. Araña, O. González Díaz, M. Miranda Saracho, J.M. Doña Rodríguez, J.A. Herrera Melián, J. Pérez Peña, Maleic acid photocatalytic degradation using Fe-TiO_2 catalysts: Dependence of the degradation mechanism on the Fe catalysts content, Appl. Catal. B 36 (2002) 113–124.

[24] V. Kumaravela, S. Mathewa, J. Bartletta, S.C. Pillai, Photocatalytic hydrogen production using metal doped TiO_2: A review of recent advances, Appl. Catal. B 244 (2019) 1021–1064.

[25] G.P. Wu, T. Chen, G.H. Zhou, X. Zong, C. Li, H_2 production with low CO selectivity from photocatalytic reforming of glucose on metal/TiO_2 catalysts, Sci. China Ser. 51 (2008) 97-100.

[26] A. Di Paola, M. Bellardita, G. Marcì, L. Palmisano, F. Parrino, R. Amadelli, Preparation of Sm-loaded brookite TiO_2 photocatalysts, Catal. Today 161 (2011) 35-40.

[27] J. Tian, X. Hu, N. Wei, Y. Zhou, X. Xu, H. Cui, H. Liu, RuO_2/TiO_2 nanobelt heterostructures with enhanced photocatalytic activity and gas-phase selective oxidation of benzyl alcohol, Sol. Energy Mater. Sol. Cells 151 (2016) 7–13.

[28] R. Fiorenza, M. Bellardita, S.Scirè, L. Palmisano, Photocatalytic H_2 production over inverse opal TiO_2 catalysts, Catal. Today 321–322 (2019) 113–119.

[29] S. Obregón, G. Colón, A ternary Er^{3+}-$BiVO_4$/TiO_2 complex heterostructure with excellent photocatalytic performance, RSC Adv. 4 (2014) 6920-6926.

[30] M. Bellardita, V. Augugliaro, V. Loddo, B. Megna, G. Palmisano, L. Palmisano, M.A. Puma, Selective oxidation of phenol and benzoic acid in water via home-prepared TiO_2 photocatalysts: distribution of hydroxylation products, Appl. Catal. A 441- 442 (2012) 79-89.

[31] D. Wang, J. Huang, F. Liu, X. Xu, X. Fang, J. Liu, Y. Xie, X. Wang, Rutile RuO_2 dispersion on rutile and anatase TiO_2 supports: The effects of support crystalline phase structure on the dispersion behaviors of the supported metal oxides, Catal. Today 339 (2020) 220–232.

[32] T.-D. Nguyen-Phan, S. Luo, D. Vovchok, J. Llorca, J. Graciani, J.F. Sanz, S. Sallis, W. Xu, J. Bai, L.F.J. Piper, D.E. Polyansky, E. Fujita, S.D. Senanayake, D.J. Stacchiola, J.A. Rodriguez, Visible light-driven H_2 production over highly dispersed ruthenia on rutile TiO_2 nanorods. ACS Catal. 6 (2016) 407– 417.

[33] J.C. Parker, R.W. Siegel, Calibration of the Raman spectrum to the oxygen stoichiometry of nanophase TiO_2, Appl. Phys. Lett. 57 (1990) 943-945.

[34] U. Balachandran, N.G. Eror, Raman spectra of titanium dioxide, J. Solid State Chem. 1982, 42, 276−282.

[35] M. Bellardita, S. Yurdakal, B.S. Tek, Ç. Değirmenci, G. Palmisano, V. Loddo, L. Palmisano, J. Soria, J. Sanz, V. Augugliaro, Tuning the selectivity to aldehyde via pH regulation in the photocatalytic oxidation of 4-methoxybenzyl alcohol and vanillyl alcohol by TiO_2 catalysts, J. Environ.l Chem. Eng. 9 (2021) 105308.

[36] A. Di Paola, M. Bellardita, R. Ceccato, L. Palmisano, F. Parrino, Highly active photocatalytic TiO_2 powders obtained by thermohydrolysis of $TiCl_4$ in water, J. Phys. Chem. C 113 (2009) 15166–15174.

[37] Z. Gao, W. Chen, X. Chen, D. Wang, S. Yi, Study on the isomerization of maleic acid to fumaric acid without catalyst, Bull. Korean Chem. Soc. 39 (2018) 920–924.

[38] Y.-C. Oh, X. Li, J.W. Cubbage, W.S. Jenks, Mechanisms of catalyst action in the TiO_2-mediated photocatalytic degradation and *cis–trans* isomerization of maleic and fumaric acid, Appl. Catal. B 54 (2004) 105–114.

[39] F. Parrino, A. Di Paola, V. Loddo, I. Pibiri, M. Bellardita, L. Palmisano, Photochemical and photocatalytic isomerization of trans-caffeic acidand cyclization of cis-caffeic acid to esculetin, Appl. Catal. B 182 (2016) 347–355.

[40] A. Masakazu, Y. Masaaki, K.Sukeya , K. Yutaka, Photocatalytic isomerization of butenes over TiO_2. Photo-formed active species and characteristics of reaction, Bull. Chem. Soc. Jpn. 1 (1986) 259-264.

[41] M.I. Franch, J.A. Ayllón, J. Peral, X. Domènech, Photocatalytic degradation of short-chain organic diacids, Catal. Today 76 (2002) 221–233.

[42] M.I. Franch, J.A. Ayllón, J. Peral, X. Domènech, Enhanced photocatalytic degradation of maleic acid by Fe(III) adsorption onto the TiO_2 surface, Catal. Today 101 (2005) 245–252.